Biosensors and Bioelectronics 162 (2020) 112273

Contents lists available at ScienceDirect

Biosensors and Bioelectronics

journal homepage: http://www.elsevier.com/locate/bios

Specific recognition of ion channel blocker by high-content cardiomyocyte electromechanical integrated correlation

Hongbo Li [a,1], Jiaru Fang [a,1], Xinwei Wei [b,1], Dongxin Xu [a,1], Tao Zhang [a], Yuting Xiang [c], Hui-Jiuan Chen [a], Fanmao Liu [a], Xi Xie [a,**], Ping Wang [b,***], Ning Hu [a,*]

[a] The First Affiliated Hospital of Sun Yat-sen University, State Key Laboratory of Optoelectronic Materials and Technologies, Guangdong Province Key Laboratory of Display Material and Technology, School of Electronics and Information Technology, Sun Yat-sen University, Guangzhou, 510006, China
[b] Biosensor National Special Laboratory, Key Laboratory of Biomedical Engineering of Ministry of Education, Department of Biomedical Engineering, Zhejiang University, Hangzhou, 310027, China
[c] The Sixth Affiliated Hospital of Sun Yat-sen University, Guangzhou, 510655, China

ARTICLE INFO

Keywords:
Cardiomyocyte-based biosensor
Electromechanical integrated correlation
Ion channel blocker
Specific recognition
Visualized analysis

ABSTRACT

Cardiac arrhythmia and drug-induced cardiotoxicity seriously threaten the human life. To develop antiarrhythmic agents and prevent the drug-induced cardiotoxicity, it is demanded to explore the high-specificity and high-efficiency drug screening platforms for preclinical investigations. Here, a specific electromechanical integrated correlation (EMIC) model was established based on the synchronized signal recording of cardiomyocyte-based biosensing system. The cardiomyocyte-based biosensing system consists of an integrated electromechanical device and a synchronized recording instrument. By extracting the feature points and correlation information of both electrical and mechanical signals, the multi-parameters of EMIC are applied for the drug recognition, showing the good specificity to analyze the typical Na^+, K^+, Ca^{2+} channel blockers. Further, visualized analysis of EMIC parameters was performed using the extracted parameters of synchronized recording signals to present the drug specific recognition functions. By heat map, radar map, and principal component analysis (PCA), the specific features and patterns were intuitively displayed to achieve the drug recognition. We believe this high-content and high-specific drug recognition strategy will be a promising and alternative method for the preclinical screening of cardiac safety and drug development in biomedical fields.

1. Introduction

Despite tremendous breakthroughs and advances in medicine and pharmaceutical science during the recent decades, cardiovascular diseases (CVDs) remain the leading cause of death all over the world (Ezzati et al., 2015; Fiuza-Luces et al., 2018; Fuster, 2014; Zhao et al., 2019), while the drug-induced cardiotoxicity is also the main reason of FDA approved drug withdrawal (Bowes et al., 2012; Ferdinandy et al., 2019; Sallam et al., 2015). Among these CVDs, cardiac arrhythmia is one of the most serious disease regardless of age, gender, and race (Ehdaie et al., 2018; Feurer et al., 2020; Shiroma and Lee, 2010), which can be characterized by the irregular electrocardiogram (ECG) coupled with abnormal contraction of heart. An acute severe arrhythmia can lead to cardiogenic shock, or even sudden death, while chronic arrhythmias may cause heart failure (Biering-Sorensen et al., 2018; McCorquodale et al., 2017). To treat the cardiac arrhythmia, antiarrhythmic agents are developed and only a small number of pharmaceuticals can finally enter the market after strict, costly, and time-consuming preclinical researches and clinical trials (Campbell and Williams, 2001; Kalyaanamoorthy and Barakat, 2018; Kumar and Zimetbaum, 2013). Most of agents serve as ion channel blockers to suppress the abnormal cardiac rhythms. However, the inhibition of human Ether-a-go-go-Related Gene (hERG)/K^+ channel blockers are proved to induce the repolarization prolongation of action potentials along with the potential early after-depolarizations (EADs) (Fermini and Fossa, 2003; Gintant et al., 2016). Therefore, the hERG channel inhibition was set as the molecular

* Corresponding author.
** Corresponding author.
*** Corresponding author.
E-mail addresses: xiexi27@mail.sysu.edu.cn (X. Xie), cnpwang@zju.edu.cn (P. Wang), huning3@mail.sysu.edu.cn (N. Hu).
[1] These authors contribute equally to this work.

https://doi.org/10.1016/j.bios.2020.112273
Received 8 April 2020; Received in revised form 29 April 2020; Accepted 2 May 2020
Available online 8 May 2020

target to screen cardiotoxicity during drug development. To improve the efficiency of drug development and avoid the later drug-induced arrhythmia, preclinical cardiac safety strategies are well established including various models and approaches. Among them, the cardiomyocyte-based model for drug preclinical test is utility and popular *in vitro* model taking throughput and clinical relevance into account (Gintant et al., 2016; Tanaka et al., 2009).

Cardiomyocyte-based model has bioinspired electrical and mechanical properties compared with heart. Both properties are associated with cardiac excitation-contraction coupling, which plays a significant role in converting electric excitation into mechanical contraction by Ca^{2+} regulation to provide the sufficient fresh blood to the whole body (Bers, 2002; Gambardella et al., 2018; Woodcock and Matkovich, 2005). Due to the importance of electrical and mechanical properties, a large number of approaches were developed to investigate the both properties of cardiomyocytes. As the gold standard technique, patch clamp is applied to study the high-quality electrophysiology of cardiomyocytes by breaking the cell membrane and forming the high seal (Cui et al., 1995). However, patch clamp technique is invasive and complicated, hampering the long-term and high-throughput recording. Besides, Ca^{2+} transients recording is another conventional method by focusing on the intracellular Ca^{2+} which reflects the mechanical contraction properties of cardiomyocytes (Cerignoli et al., 2012; Dittami et al., 2011; Maxwell and Blatter, 2017). However, this label-based biosensing technology suffers the phototoxicity and drug adverse effect, which significantly affect the cell viability and limit the chronic recording (Carpenter-Deyo et al., 1991; Icha et al., 2017). To perform the high-throughput, long--term electrical and mechanical recording of cardiomyocytes, non-invasive, label-free cell-based biosensor technologies were well developed for cardiomyocyte physiology investigation and drug

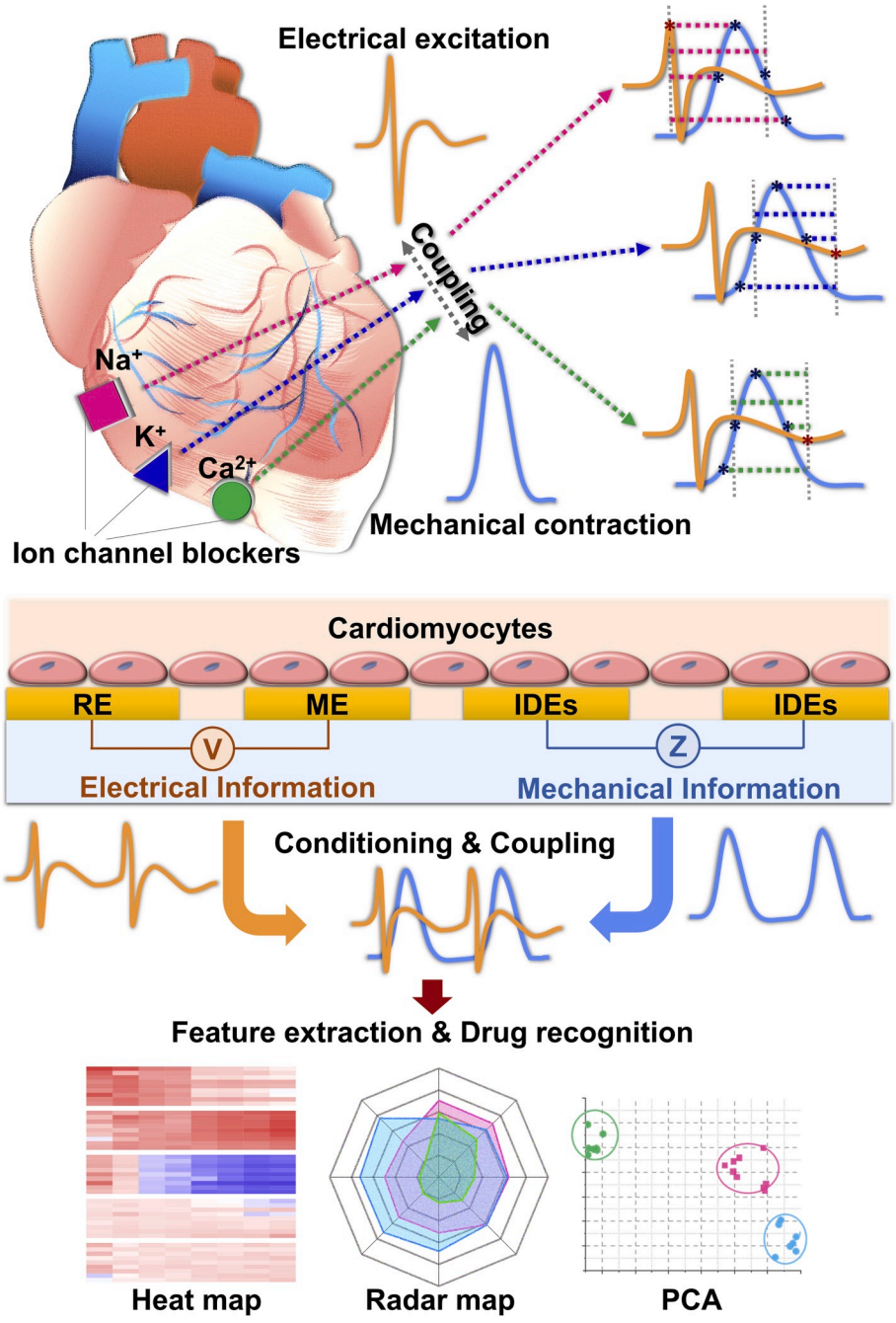

Fig. 1. Schematic of drug specific recognition by high-content cardiomyocyte electromechanical integrated correlation. The synchronized biosensing system collects the electrical and mechanical information of cardiomyocytes by microelectrodes (ME), reference electrode (RE), and interdigitated electrodes (IDEs). The electrical and mechanical signals are initially conditioned by amplification and filtering of conditioning circuit before signal acquisition. The conditioned electrical and mechanical signals are then coupled by synchronous signal acquisition and analysis to establish the electromechanical integrated correlation. The electromechanical integrated correlation (EMIC) model is developed by feature extraction, and the visualized drug specific recognition model is established in the form of heat map, radar map, and principal component analysis (PCA).

analysis. Microelectrode arrays (MEAs) or Complementary Metal-Oxide-Semiconductor Transistor (CMOS) were broadly employed to study the extracellular information (Clements, 2016; Clements and Thomas, 2014; Park et al., 2019). Meanwhile, interdigitated electrodes (IDEs) and cantilever-shape piezoresistive sensors were reported to measure the mechanical contraction of cardiomyocytes, focusing on the drug-induced mechanical changes (Kim et al., 2016, 2017; Wang et al., 2013).

The electrical and mechanical properties are related to the ion channel activities of cardiomyocytes, so the cardiomyocytes-based electrical and mechanical biosensors were established to study ion channel blockers. The parameters of electrical signals can reflect the effects of ion channel blockers by spike amplitude, action potential duration, and firing rate (Dipalo et al., 2018; Park et al., 2019; Wang

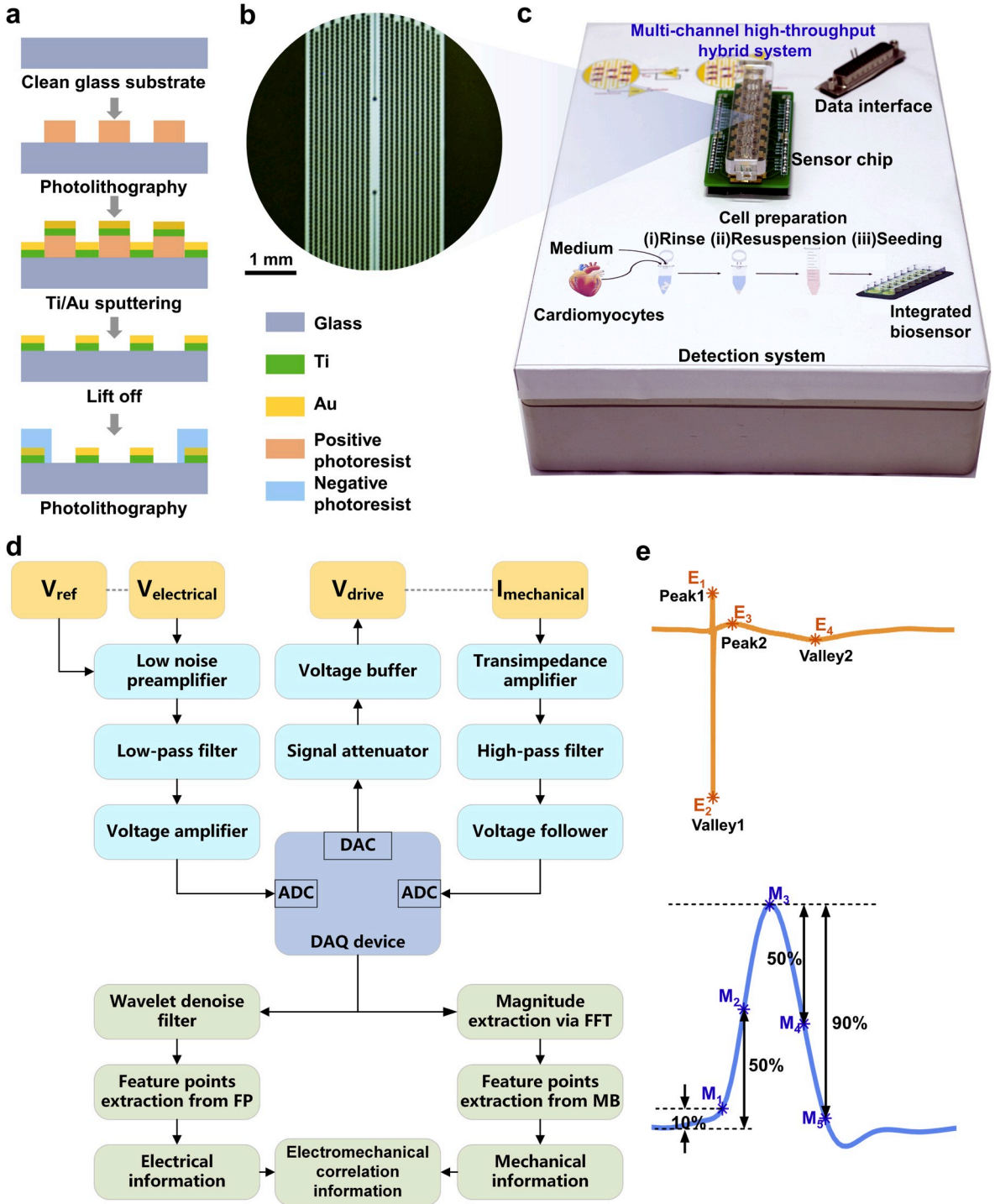

Fig. 2. Design of electromechanical integrated cardiomyocyte-based biosensing system. (a) The fabrication procedures of integrated cell-based biosensor with IDEs and MEs. (b) Optical image of integrated cardiomyocyte-based biosensor with IDEs and MEs. (c) Pictures of detection system for signals measurement. (d) Block diagram of biosensing system including signal generation module (orange), analog signal conditioning module (cyan), digital-to-analog convertor (DAC) and analog-to-digital convertor (ADC) integrated data acquisition (DAQ) module, and the software signal processing module (gray). (e) Demonstration of electrical (E) and mechanical (M) feature points extracted from field potential (FP) and mechanical beating (MB) signals. (For interpretation of the references to colour in this figure legend, the reader is referred to the Web version of this article.)

et al., 2015). Meanwhile, the parameters of mechanical signals can reflect the effects of ion channel blockers by amplitude, duration, and rate of mechanical beating signals (Caluori et al., 2019; Hu et al., 2015; Kim et al., 2016, 2020). Though the electromechanical integrated devices and methods are ready for simultaneous multiparameter recording of cardiomyocytes, the drug screening is still based on individual parameter analysis of electrical or mechanical signals (Doerr et al., 2015; Guo et al., 2011; Herron et al., 2012; Hu et al., 2018; Kehat et al., 2004). Cardiomyocyte electromechanical integrated correlation is conventionally ignored to study the ion channel blockers.

Here, we proposed a specific recognition strategy of ion channel blockers by high-content cardiomyocyte electromechanical integrated correlation (EMIC) (Fig. 1). The strategy was established by the ion channel blocker effect on corresponding ion channels on the cardiomyocytes. The inhibition of specific ion channel directly affected the specific parameters of electrical signals, and subsequently induced the specific changes of mechanical contraction based on the excitation-contraction coupling, so the changes of electromechanical integrated correlation can be derived and analyzed for specific recognition of ion channel blockers. To established the EMIC model, a synchronized electromechanical integrated cardiomyocyte-based biosensing system was developed. To perform the electromechanical integrated recording, IDEs and microelectrodes (MEs) are integrated on the same device, while the matched recording system is also developed. The unique drug recognition strategy can provide high-content information about drug-induced excitation-contraction coupling changes of cardiomyocytes. By determining the feature points (E and M) from the electrical and mechanical signal profiles, and EMIC model parameters can be subsequently calculated and optimized. By treatment of typical ion channel blockers, the specific changes of selected EMIC model parameters could be further collected, showing the specific responses to blockers. Finally, visualized specific recognition models of ion channels blockers were established. We believe this new recognition strategy will be a promising and alternative method for the preclinical drug screening.

2. Experimental and methods

2.1. Device fabrication

The device is fabricated on a 4-inch quartz glass wafer (Corning, USA) by integrating IDEs and MEs. The fabrication procedures are shown in Fig. 2a. After spin coating, UV exposure and development, positive photoresist Microposit S1813 (Kayaku Advanced Materials, USA) was patterned on the substrate. 5 nm Ti/100 nm Au pattern were then fabricated by sputtering and lift-off processes. The leads of IDEs and MEs were insulated by negative photoresist SU-8 2002 (Kayaku Advanced Materials, USA) to finish the fabrication. Two MEs with 100 μm in diameter and 2 mm in center-to-center spacing were designed between two symmetrical IDEs with 120 μm center-to-center spacing circle-on-line branches, and the reference electrodes are designed at the edge of IDEs (Fig. 2b). The device is finally assembled on a customized polymethyl methacrylate (PMMA) chamber for cell culture.

2.2. Detection principle of EMIC signals

The integrated sensor was designed to record the electrical and mechanical signals of cardiomyocyte. MEs can record the extracellular potentials of cardiomyocytes after cells attach and mature on the MEs. The extracellular potential originates from the action potential induced by Na^+, K^+, and Ca^{2+} current. Meanwhile, IDEs was designed to record the mechanical signals by electric cell-substrate impedance sensing (ECIS). When alternating current (AC) voltage with featured frequency is applied on the IDEs, a stable ion current will generate between the paired IDEs with the same frequency (Ye et al., 2019; Zhang et al., 2018). This current fluctuates by the rhythmic mechanical contraction of cardiomyocytes due to changes of cell morphology and cell-electrode attachment, resulting in impedance changes of IDEs. Combining two types of sensor, the integrated device can collect both electrical and mechanical information of cardiomyocytes.

2.3. Development of synchronized recording system

The block diagram of the analog circuit functional module is shown in Fig. 2d in cyan. Based on different working principles of IDEs and MEs, the analog signal conditioning module simultaneously processed the electrical signal $V_{electrical}$ and mechanical signal $I_{mechanical}$ induced by cardiomyocytes. To convert the weak field potential (FP) of cardiomyocytes (with an amplitude ranging from 100 μV to 2 mV) into high-quality signals for acquisition, FP signals are pre-amplified (Gain = 20) and then filtered by R-C high-pass passive filter (with a cut-off frequency of 0.5 Hz) to remove the baseline drift. To remove the high-frequent noise, Butterworth low-pass active filter (with a cut-off frequency of 3 kHz) and secondary amplification (Gain = 50) are subsequently employed. The 3 kHz low-pass filter can effectively remove the high-frequency (typically 10 kHz) AC drive signal of IDEs from the FP signals, which is the key design for the synchronized recording of FP and MB signals. Finally, the optimized FP signals are transmitted to analog-to-digital converter (ADC) of DAQ device. On the other hand, mechanical beating (MB) signals are derived from the impedance changes of IDEs under a sensitive frequency (10 kHz). In contrast to the passive MEs, the active IDEs require the AC drive signal which is provided by digital-to-analog converter (DAC) of DAQ device. By signal attenuation and buffering modules, a high-quality AC drive signals (30 mV in amplitude) with strong drive ability are applied to one end of IDEs, and AC currents will outflow from the paired end. This current signal will be converted into AC voltage signals by a transimpedance amplifier (TIA). The voltage signals are then conditioned by high-pass amplifier and voltage follower module. MB signals are also transmitted to analog-to to-digital converter (ADC) of DAQ device. Thus, both FP and MB signals can be synchronously collected by the DAQ device.

2.4. Digital signal processing and feature extraction

The subsequent signal processing and feature extraction is operated in customized LabVIEW program (National Instrument, USA). To remove the noise and avoid loss of signal features, undecimated wavelet transform (UWT) are applied for denoising (Appathurai et al., 2019; Sundarasekar et al., 2018). On the other hand, the MB signals are calculated from the recorded AC signals by Fast Fourier Transform (FFT) algorithm. MB signals are detrended and presented in the form of changed impedance-to-background impedance magnitude ratio ($|\triangle Z|/|Z_0|$) in percentage. After denoising both signals, feature points are extracted from FP and MB signals by the adaptive threshold algorithm, respectively. Shown in Fig. 2e, based on the features of FP signals, maximum and minimum points of first signal peak in FP are labeled as E1 and E2, and the maximum and falling end points of second signal peak in FP are labeled as E3 and E4. Based on the features of MB signals, the rising 10%, rising 50%, maximum, falling 50%, and falling 90% points of in MB were labeled as M1, M2, M3, M4, and M5, respectively. These feature points from both signals were applied to calculate the parameters of EMIC to perform the further correlation analysis.

2.5. Cardiomyocyte culture and drug assay

Human induced pluripotent stem cell derived cardiomyocytes (hiPSC-CMs), Cor.4U cardiomyocytes (Ncardia, Germany) are employed as the *in vitro* cell model for synchronized system test and drug assay. To improve the cell-substrate attachment, devices are coated with 50 μL fibronectin diluted solution (10 mg/mL) in phosphate buffer solution (PBS) without Ca^{2+}/Mg^{2+} in the incubator (37 °C, 5.0% CO_2) overnight. After cardiomyocytes are thawed and seeded in the device with a density of 25,000 cells/well, the cardiomyocyte-based biosensors are fixed on

the synchronized recording system and kept in the incubator, and the medium is changed every two days. Then, electrical and mechanical signals are continuously recorded by this system in a label-free and dynamic manner for several weeks, and the drug assays are carried out when the cardiomyocytes present the mature FP and MB signals. In the drug assays, deionized water (H_2O) and 0.1% dimethylsulfoxide (DMSO) were set as control group to evaluate the effect of general pharmaceutical solvents, while the typical ion channel blockers e.g., lidocaine (Na^+), E−4031(K^+) and isradipine (Ca^{2+}) (Sigma-Aldrich, USA) were chosen for drug test. All compounds were prepared by culture medium and heated to 37 °C before drug assays.

2.6. Data analysis

Signal processing and principal components analysis (PCA) was operated by customized LabVIEW program. All statistical analysis was performed using Prism 8.0 (GraphPad, USA) and SPSS 10.0 (SPSS Inc., USA), and the results are presented as mean ± SD (standard deviation).

3. Results and discussion

3.1. Establishment and optimization of cardiomyocyte EMIC model

To establish the human-specific cardiomyocyte EMIC model, hiPSC-CMs were employed to construct the cell-based biosensing system. Cardiomyocytes were first cultured on the integrated device with an optimal density (Fig. 3a). The hiPSC-CMs can be cultured for several weeks *in vitro*. Generally, the synchronized FP and MB signals can be recorded after 2-day culture, which were defined as EMIC signals, and the synchronized recording signals present high and stable quality after 4–5 days, which is suitable to perform the following assays. As shown in Fig. 3b, the representative EMIC signals contained both rhythmic FP (orange) and MB signals (blue), and MB signals generally follow FP signals with the same rhythm based on the excitation-contraction coupling. From the partial enlarged synchronize recording signal (red dash box in Fig. 3b), it can be found two peaks (the sharp and the gentle) in FP and one peak in MB (Fig. 3c). Based on the profiles of FP and MB signals, the feature E1 to E4 and M1 to M5 points were extracted from both signals by customized LabVIEW program, which can help to analyze the EMIC information. The EMIC parameters were then derived and calculated by the time intervals between E and M feature points. The functional feature points can be further determined by data analysis E1 was close to E2, so only E1 was selected. Consequently, taking the into account, E1, E3, E4, M1 to M5 are finally employed to establish the EMIC model by analyzing the temporal correlation. The EMIC model was based on the excitation-contraction coupling of cardiomyocytes which refers to a series of events linking electric activity to mechanical activity (Bers, 2002; Mayourian et al., 2018; van Meer et al., 2019). Therefore, this EMIC information contained the high-content correlation between electric and mechanical behaviors.

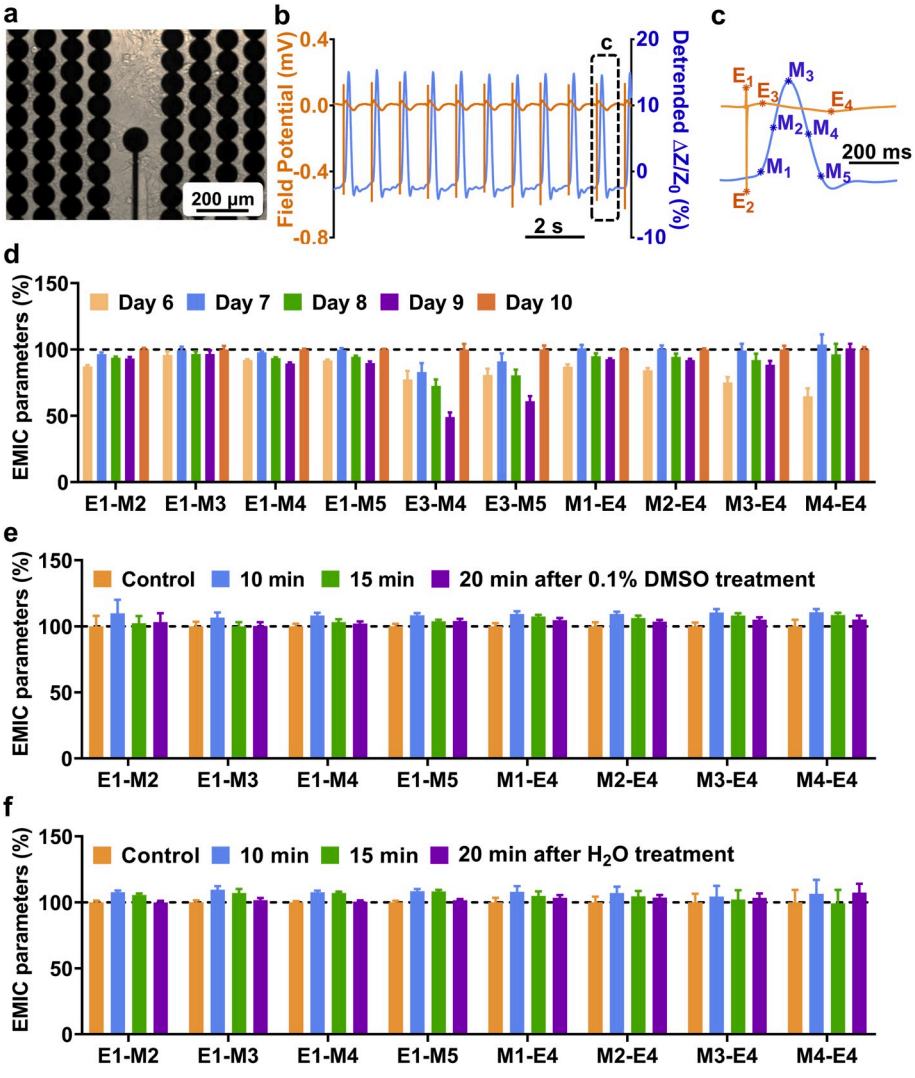

Fig. 3. Establishment and optimization of electro-mechanical integrated correlation (EMIC) model. (a) Optical image of cardiomyocytes on the integrated device. (b) Typical EMIC profiles involving the field potential (orange) and mechanical beating (blue) signals. (c) Partial enlarged signals in red dash box of (b) with defined feature points. (d) Long-term stability analysis of typical EMIC parameters from day 6–10 (n = 9). (e) The stability analysis of selected EMIC parameters under H_2O treatment (n = 9). (f) The stability analysis of selected EMIC parameters under dimethylsulfoxide (DMSO) treatment (n = 9). (For interpretation of the references to colour in this figure legend, the reader is referred to the Web version of this article.)

To optimize the EMIC model, the long-term and solvent stability of EMIC parameters were examined, respectively. For the long-term stability analysis, the EMIC parameters from day 6–10 were selected. From the analysis results of EMIC parameters during, 8 of EMIC parameters (E1-M2, E1-M3, E1-M4, E1-M5, M1-E4, M2-E4, M3-E4, and M4-E4) were stable from day 7 with small differences within 15%, while E3-M4 and M3-E5 presented a large fluctuation during day 7 to day 10 (Fig. 3d), so the E3 feature point were excluded. E1, E4, M1 to M5 are further selected to establish the EMIC parameters. After the long-term stability optimization, the solvent side effect was also tested before drug assays. H_2O and DMSO are the common solvent, so their impact on the EMIC model was also evaluated for the further drug tests. 10, 15, 20 min solvent treatment are analyzed. Compared to control group, H_2O and 0.1% DMSO presented the slight influence on EMIC model after 10–20 min treatment. As shown in Fig. 3d and e, the maximum difference induced by H_2O was 9.62% (10 min treatment for E1-M3), while the maximum difference induced by 0.1% DMSO was 9.85% (10 min treatment for E1-M2) and gradually decreased as reported (Hyun et al., 2017). It indicated that the selected parameters of EMIC model were relative stable and reliable for further drug treatment in DMSO solvent. Based on the long-term and solvent stability test, DMSO solvent could be used in the following drug assay.

3.2. Ion channel drug evaluation of EMIC model

EMIC model is established on the basis of the cardiomyocyte excitation-contraction behavior, so it was highly related to Na^+, K^+, and Ca^{2+} channels (Grant, 2009). To investigate ion channel related responses of EMIC model, three typical ion channel drugs, lidocaine (Na^+ channel blocker), E−4031 (K^+ channel blocker), and isradipine (Ca^{2+} channel blocker) were applied to treat the cardiomyocyte-based biosensing system, and the EMIC model can be further tested by these drugs. Based on the optimal EMIC parameters, the drug effects on the EMIC model can be tested by the high-content analysis.

Synchronized recording signals were analyzed after 10 min drug treatment. Representative EMIC model response to lidocaine (a Na^+ channel blocker) were shown in Fig. 4a–c. From the signal analysis, it was obviously seen that the E1-M prolonged. Taking the solvent fluctuation responses (9.62% for H_2O and 9.85% for 0.1% DMSO) into account, the increase percentage of E1-M2 (38.06%), E1-M3 (37.04%), E1-M4 (29.90%), E1-M5 (27.12%), M1-E4 (13.89%), M2-E4 (14.93%), and M3-E4 (12.10%) were considered as the effective response of EMIC model. Due to the lidocaine inhibits the Na^+ channels and slow the signal conduction (Lee et al., 2018), the delay of signal conduction could affect all the cultured cardiomyocytes, which was reflected by increase of mechanical beating duration, so the interval between the field potential and mechanical beating increase, leading to sharp increase of EMIC model parameters, E1-M2, E1-M3, E1-M4, and E1-M5.

For K^+ channel blocker test, E−4031 was employed to treat the cardiomyocyte-based biosensing system, and representative EMIC model response to E−4031 were presented in Fig. 4d–f. Taking the solvent fluctuation response into account, the increase percentage of E1-M2 (27.68%), E1-M3 (18.40%), E1-M4 (14.22%), E1-M5 (17.32%), M1-E4 (44.08%), M2-E4 (45.92%), M3-E4 (53.58%), and M4-E4 (82.28%) were considered as the effective response of EMIC model in the presence of E−4031 (a K^+ channel blocker). E−4031 inhibits the K^+ channels and delays the inactivation of Ca^{2+} channels, leading to the prolongation of repolarization (Follmer and Colatsky, 1990), so the E1-M2, E1-M3, E1-M4, M2-E4, M3-E4, and M4-E4 increased due to the prolongation of Ca^{2+} inflow, while the repolarization endpoint (E4) of field potential was also delayed. Though both mechanical beating duration (M1-M5) and field potential duration (E1-E4) prolonged, the mechanical beating

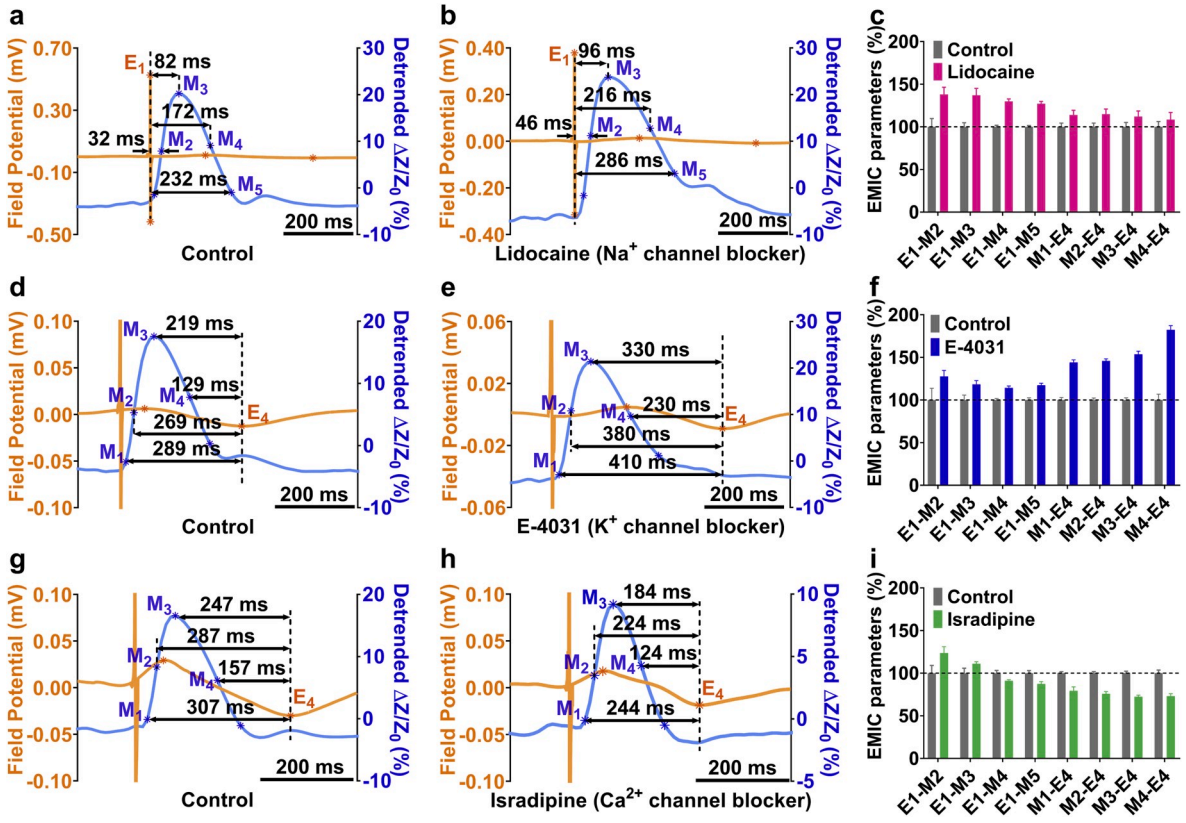

Fig. 4. Electromechanical integrated correlation (EMIC) model for ion channel blocker evaluation. (a–b) Typical EMIC model responses to the lidocaine (Na^+ channel blocker) treatment. (c) Statistical analysis of selected EMIC model parameters induced by lidocaine (n = 9). (d–e) Typical EMIC model responses to the E−4031 (K^+ channel blocker) treatment. (f) Statistical analysis of selected EMIC model parameters induced by E−4031 (n = 9). (g–h) Typical EMIC model responses to the isradipine (Ca^{2+} channel blocker) treatment. (i) Statistical analysis of selected EMIC model parameters induced by isradipine (n = 9).

duration (M1-M5) increases by 15.51% from the 207.78 ± 4.16 ms to 240.00 ± 4.71 ms, which was significantly less than increase (43.72% from the 306.69 ± 9.41 ms to 440.78 ± 5.94 ms) of the field potential duration (E1-E4) due to K^+ channel blocker induced significant repolarization prolongation. Therefore, the M1-E4, M2-E4, M3-E4, and M4-E4 of EMIC model were increased significantly.

After the Na^+ and K^+ channel blocker (lidocaine and E−4031) tests, the isradipine (a Ca^{2+} channel blocker) was employed to test the EMIC model of cardiomyocyte-based biosensing system. Compared with the Na^+ and K^+ channel blockers, Ca^{2+} channel blocker (isradipine) induced the obviously different EMIC model responses (Fig. 4g–i). From the statistical analysis, E1-M2 (23.60%), E1-M3 (11.06%), E1-M5 (−12.64%), M1-E4 (−20.67%), M2-E4 (−24.17%), M3-E4 (−27.61%), and M4-E4 (−26.92%) were considered as the effective response of EMIC model. Isradipine can shorten the action potential duration by inhibiting the Ca^{2+} channel and affect the signal conduction (Epstein and Braunwald, 1982), so EMIC parameters E1-M2 increased. Besides, due to the inhibition of Ca^{2+} channel, mechanical beating will end soon and its duration (M1-M5) was shortened by 23.86 ms from 197.78 ± 4.91 ms to 163.82 ± 7.68 ms, while the field potential duration was significantly shortened by 56.75 ms from 333.13 ± 5.90 ms to 277.38 ± 7.20 ms. Therefore, M1-E4, M2-E4, M3-E4, and M4-E4 significantly decreased.

This unique model was mainly based on ion channels, which played a key role in the electrophysiological activities of cardiomyocytes and affects both the action potential and the corresponding mechanical contraction. By the tests of Na^+, K^+, Ca^{2+} ion channel blocker, the E-M parameters of EMIC model present the specific response to these typical ion channel blockers, which could be potentially applied for the further drug specific recognition. The unique responses highly relied on the synchronized recording function of the cardiomyocyte-based biosensing system, which was difficult to achieve by asynchronous or individual systems. With the assistance of characteristic EMIC parameters, changes in paired FP and MB synchronized recording signals can be clearly revealed for better understanding of the special electromechanical integrated activity in a high-content manner.

3.3. Specific recognition of ion channel blockers

To further improve the specific recognition for ion channel blockers, visualized functions were developed in the EMIC model to improve the visualization and analysis efficiency. The heat map, radar map, and PCA were introduced to visualize the EMIC parameters. In the heat map as shown in Fig. 5a, the model specific responses to each ion channel blocker were obvious compared with the control group (H_2O and DMSO). The regions of H_2O and DMSO are almost in white which indicates the solvents have seldom impact (within ±10%) on EMIC model parameters. Meanwhile, the ion channel blockers led to different appearances corresponding to the above statistical analysis. Based on the change ratio from the synchronized signal analysis, E1-M2, E1-M3, E1-M4, E1-M5 of Na^+ blocker region is in dark red showing the large and specific changes in these EMIC parameters. M1-E4, M2-E4, M3-E4, M4-E4 of K^+ blocker region presents dark red which indicated the large and specific changes in these EMIC parameters. In contrast to Na^+ and K^+ blockers, the M1-E4, M2-E4, M3-E4, and M4-E4 of Ca^{2+} region is in dark blue, which implied the large decrease of these EMIC parameters.

Moreover, the radar map or called spider diagram was also introduced to provide an alternative mean to present the differences under treatment of these compounds (Fig. 5b). Using the radar map, all the EMIC parameters can be integrated for comparison in one map, and the parameters can be set at defined corners, and the corners of 100% dashed octagon is control group for each treatment. H_2O and DMSO solvent groups presented small spread after the treatment, which also visually reflected the results of the solvent stability. Na^+ blocker treatment group showed the significant spread at E1-M2, E1-M3, E1-M4, and E1-M5, while K^+ blocker treatment group presented the significant

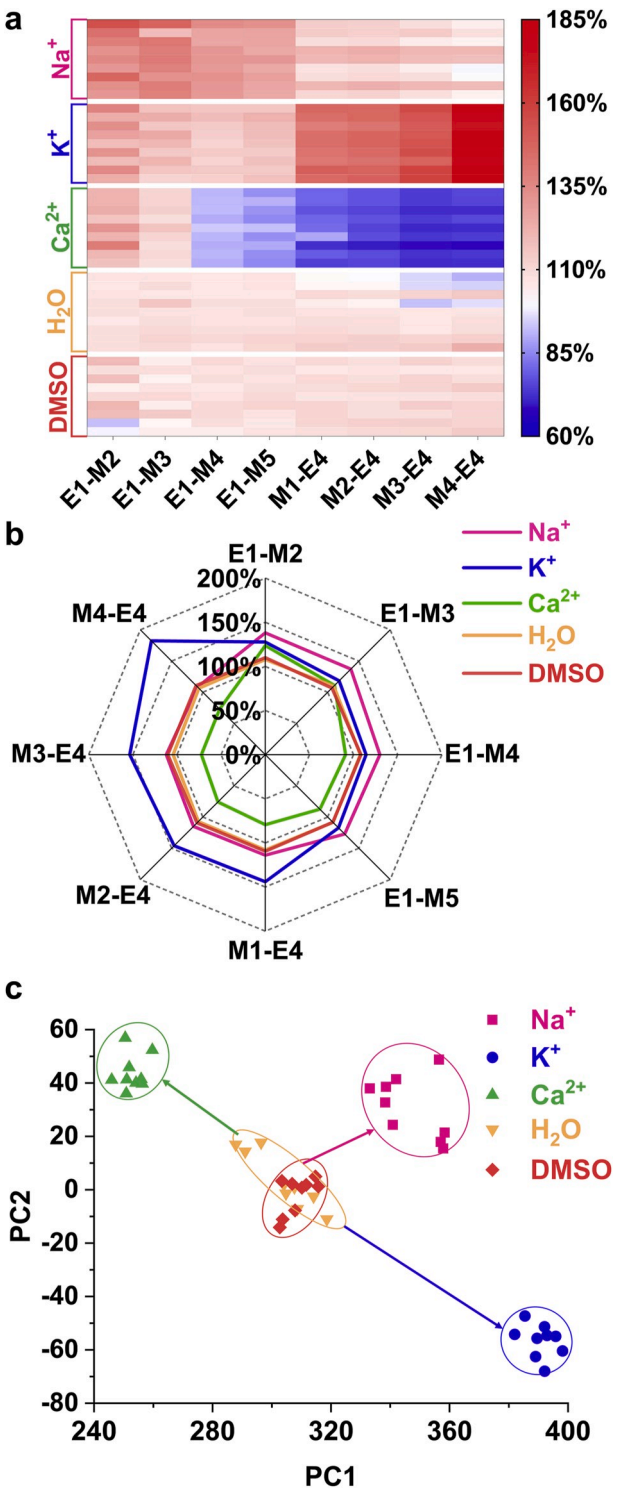

Fig. 5. Ion channel blocker specific recognition. (a) Heat map of characteristic electromechanical integrated correlation (EMIC) model parameters after treatment of Na^+ channel blocker (Na^+), K^+ channel blocker (K^+), Ca^{2+} channel blocker (Ca^{2+}), H_2O, and dimethylsulfoxide (DMSO). In heat map, the regions of H_2O and DMSO are almost in white which indicates the solvents have seldom impact (within ±10%) on EMIC model, while the ion channel blockers led to specific appearance corresponding to the statistical analysis. (b) Radar map for ion channel blockers specific recognition. In radar map, three blockers presented their specific patterns compared with the control groups (c) Principal component analysis (PCA) based clustering results. The three types of ion channel blockers are far away from each other, indicating their specific parameters of EMIC model.

spread at E1-M2, M1-E4, M2-E4, M3-E4, and M4-E4. Ca^{2+} blocker in the radar map showed the shrink pattern at M1-E4, M2-E4, M3-E4, M4-E4 and the spread pattern at E1-M2. In the radar map, each ion channel blocker had its specific pattern compared with the control patterns, and it can intuitively reflect visualization responses of EMIC model.

Furthermore, to perform the visualized clustering analysis, PCA algorithm was also employed for establishment visualized EMIC model for the ion channel blockers recognition. All data were clustered into five regions, where regions of H_2O and DMSO are close to each other, while regions of Na^+, K^+, and Ca^{2+} were non-overlapping and far from the regions of H_2O and DMSO (Fig. 5c). The weight coefficients of PC1 and PC2 are 98.63% and 1.21% in the PCA analysis. The average Euclidean distances from Na^+, K^+, and Ca^{2+} blocker regions to H_2O region were 51.33, 105.73, and 64.92, respectively, which are significantly farther than that from DMSO region to H_2O region (7.27). The analysis results indicate that EMIC model can specifically recognize the Na^+, K^+, and Ca^{2+} channel blockers by visualized PCA patterns.

The ion channels on the membrane of cardiomyocyte play a significant role, which are also important drug targets. Under the ion channel blocker treatments, the action potentials of cardiomyocytes are affected, which subsequently disturbs their mechanical contraction behavior. In contrast to the conventional individual analysis, the EMIC model was established by temporal analysis of synchronized recording signals. This EMIC model can not only explore the temporal electromechanical integrated parameters for drug analysis, but provide the multiple visualized specific recognition methods and patterns as well. The versatile EMIC model will be a promising and alternative strategy for the specific recognition of drug efficacy in the biomedical and pharmaceutical field.

4. Conclusion and perspectives

In this study, a specific recognition EMIC model for ion channel blockers was established based on the synchronized signal recording of cardiomyocyte-based biosensing system, which focused on the temporal correlation between electrical and mechanical information of cardiomyocytes. The stable EMIC model was built via extraction, analysis, and optimization of EMIC parameters involving factors of cardiomyocyte growth and solvent. Moreover, specific temporal correlation responses of EMIC model induced by Na^+, K^+, and Ca^{2+} channel blockers were investigated EMIC signal profiles and statistical analysis. Furthermore, to improve the readability and practicality, data visualization was introduced by heat map and radar map to present visualized overview of EMIC model. Finally, a specific recognition model of ion channel blockers was built by PCA algorithm, which provided a quantitative and utility method for preclinical practices.

The advantages of high-throughput, non-invasiveness, visualization, and digitization make the EMIC model suitable for the high-content, efficient, and reliable screening during preclinical drug study. Due to the high-performance of EMIC model, the specific recognition method of ion channel blockers may provide the alternative evidence and efficient approach to develop antiarrhythmic drugs and drug safety screening. With the accumulation of data, a comprehensive drug specific recognition EMIC model could be established as a promising tool in cardiology or pharmacology field to help defend CVDs and promote human health.

Declaration of competing interest

The authors declare that they have no known competing financial interests or personal relationships that could have appeared to influence the work reported in this paper.

CRediT authorship contribution statement

Hongbo Li: Conceptualization, Investigation, Writing - original draft, Writing - review & editing, Visualization. **Jiaru Fang:** Investigation, Methodology, Writing - original draft. **Xinwei Wei:** Software, Formal analysis, Writing - original draft. **Dongxin Xu:** Investigation, Validation, Writing - original draft. **Tao Zhang:** Methodology, Software, Data curation. **Yuting Xiang:** Writing - review & editing. **Hui-Jiuan Chen:** Resources, Writing - review & editing, Funding acquisition. **Fanmao Liu:** Resources, Writing - review & editing, Funding acquisition. **Xi Xie:** Conceptualization, Writing - review & editing, Supervision, Project administration, Funding acquisition. **Ping Wang:** Conceptualization, Writing - review & editing, Supervision, Project administration, Funding acquisition. **Ning Hu:** Conceptualization, Writing - original draft, Writing - review & editing, Supervision, Project administration, Funding acquisition.

Acknowledgements

The work is supported in part by the National Natural Science Foundation of China (Grant Nos. 61771498, 31627801, 61901535, 31900954), and Guangdong Basic and Applied Basic Research Foundation (Grant No. 2020A1515010665, 2019A1515012087). The authors wish to thank the Youth 1000 Talents Program of China, 100 Talents Program of Sun Yat-Sen University (Grant Nos. 76120-18841213, 76120-18821104), and Basic Scientific Research Special Foundation of Sun Yat-Sen University (Grant Nos. 20lgpy47, 20lgzd14).

References

Appathurai, A., Jerusalin Carol, J., Raja, C., Kumar, S.N., Daniel, A.V., Jasmine Gnana Malar, A., Fred, A.L., Krishnamoorthy, S., 2019. Measurement 147, 106384.
Bers, D.M., 2002. Nature 415, 198–205.
Biering-Sorensen, T., Kabir, M., Waks, J.W., Thomas, J., Post, W.S., Soliman, E.Z., Buxton, A.E., Shah, A.M., Solomon, S.D., Tereshchenko, L.G., 2018. Circ. Arrhythmia Elec 11 (3), e005961.
Bowes, J., Brown, A.J., Hamon, J., Jarolimek, W., Sridhar, A., Waldron, G., Whitebread, S., 2012. Nat. Rev. Drug Discov. 11 (12), 909–922.
Caluori, G., Pribyl, J., Pesl, M., Jelinkova, S., Rotrekl, V., Skladal, P., Raiteri, R., 2019. Biosens. Bioelectron. 124–125, 129–135.
Campbell, T., Williams, K., 2001. Br. J. Clin. Pharmacol. 52 (S1), 21–33.
Carpenter-Deyo, L., Duimstra, J.R., Hedstrom, O., Reed, D.J., 1991. J. Pharmacol. Exp. Therapeut. 258 (2), 739–746.
Cerignoli, F., Charlot, D., Whittaker, R., Ingermanson, R., Gehalot, P., Savchenko, A., Gallacher, D.J., Towart, R., Price, J.H., McDonough, P.M., Mercola, M., 2012. J. Pharmacol. Toxicol. Methods 66 (3), 246–256.
Clements, M., 2016. Curr. Protoc. Toxicol. 68, 22.24.1-22.4.32.
Clements, M., Thomas, N., 2014. Toxicol. Sci. 140 (2), 445–461.
Cui, C., Smith, D., Adler, J., 1995. J. Membr. Biol. 144 (1), 31–42.
Dipalo, M., Melle, G., Lovato, L., Jacassi, A., Santoro, F., Caprettini, V., Schirato, A., Alabastri, A., Garoli, D., Bruno, G., Tantussi, F., De Angelis, F., 2018. Nat. Nanotechnol. 13 (10), 965–971.
Dittami, G.M., Rajguru, S.M., Lasher, R.A., Hitchcock, R.W., Rabbitt, R.D., 2011. J. Physiol. 589 (6), 1295–1306.
Doerr, L., Thomas, U., Guinot, D.R., Bot, C.T., Stoelzle-Feix, S., Beckler, M., George, M., Fertig, N., 2015. J. Lab. Autom. 20 (2), 175–188.
Ehdaie, A., Cingolani, E., Shehata, M., Wang, X., Curtis, A.B., Chugh, S.S., 2018. Circ. Arrhythmia Elec 11 (3), e005680.
Epstein, F.H., Braunwald, E., 1982. N. Engl. J. Med. 307 (26), 1618–1627.
Ezzati, M., Obermeyer, Z., Tzoulaki, I., Mayosi, B.M., Elliott, P., Leon, D.A., 2015. Nat. Rev. Cardiol. 12 (9), 508–530.
Ferdinandy, P., Baczko, I., Bencsik, P., Giricz, Z., Gorbe, A., Pacher, P., Varga, Z.V., Varro, A., Schulz, R., 2019. Eur. Heart J. 40 (22), 1771–1777.
Fermini, B., Fossa, A.A., 2003. Nat. Rev. Drug Discov. 2 (6), 439–447.
Feurer, C., Woody, M.L., James, K.M., Kudinova, A.Y., Gibb, B.E., 2020. Dev. Psychobiol. 62 (2), 232–239.
Fiuza-Luces, C., Santos-Lozano, A., Joyner, M., Carrera-Bastos, P., Picazo, O., Zugaza, J. L., Izquierdo, M., Ruilope, L.M., Lucia, A., 2018. Nat. Rev. Cardiol. 15 (12), 731–743.
Follmer, C., Colatsky, T., 1990. Circulation 82 (1), 289–293.
Fuster, V., 2014. Nat. Rev. Cardiol. 11 (11), 671–683.
Gambardella, J., Trimarco, B., Iaccarino, G., Santulli, G., 2018. Adv. Exp. Med. Biol. 1067, 373–385.
Gintant, G., Sager, P.T., Stockbridge, N., 2016. Nat. Rev. Drug Discov. 15 (7), 457–471.
Grant, A.O., 2009. Circ. Arrhythmia Elec 2 (2), 185–194.
Guo, L., Abrams, R., Babiarz, J.E., Cohen, J.D., Kameoka, S., Sanders, M.J., Chiao, E., Kolaja, K.L., 2011. Toxicol. Sci. 123, 281–289.
Herron, T.J., Lee, P., Jalife, J., 2012. Circ. Res. 110 (4), 609–623.
Hu, N., Wang, T., Wan, H., Zhuang, L., Kettenhofen, R., Zhang, X., Zhang, Y.S., Xu, W., Gossmann, M., Bohlen, H., Hou, X., Wang, P., 2018. Biosens. Bioelectron. 117, 354–365.
Hu, N., Wang, T., Wang, Q., Zhou, J., Zou, L., Su, K., Wu, J., Wang, P., 2015. Biosens. Bioelectron. 67, 146–153.

Hyun, S.W., Kim, B.R., Hyun, S.A., Seo, J.W., 2017. J. Pharmacol. Toxicol. Methods 87, 93–98.
Icha, J., Weber, M., Waters, J.C., Norden, C., 2017. Bioessays 39 (8), 1700003.
Kalyaanamoorthy, S., Barakat, K.H., 2018. Med. Res. Rev. 38 (2), 525–555.
Kehat, I., Khimovich, L., Caspi, O., Gepstein, A., Shofti, R., Arbel, G., Huber, I., Satin, J., Itskovitz-Eldor, J., Gepstein, L., 2004. Nat. Biotechnol. 22 (10), 1282–1289.
Kim, D., Choi, Y., Shanmugasundaram, A., Jeong, Y., Park, J., Oyunbaatar, N., Kim, E., Choi, M., Lee, D., 2020. Nat. Commun. 11 (1), 535.
Kim, D., Jeong, Y., Lee, B., Shanmugasundaram, A., Lee, D., 2017. Sensor. Actuator. B Chem. 240, 566–572.
Kim, J., Choi, Y., Lee, B., Lee, D., 2016. Biosens. Bioelectron. 80, 456–462.
Kumar, K., Zimetbaum, P.J., 2013. Curr. Cardiol. Rep. 15 (10), 410.
Lee, H., Hyun, S., Byun, B., Chae, J., Kim, K., 2018. PloS One 13 (4), e0195577.
Maxwell, J.T., Blatter, L.A., 2017. J. Physiol. 595 (12), 3835–3845.
Mayourian, J., Ceholski, D.K., Gonzalez, D.M., Cashman, T.J., Sahoo, S., Hajjar, R.J., Costa, K.D., 2018. Circ. Res. 122 (1), 167–183.
McCorquodale, A., Poulton, R., Hendry, J., Norrish, G., Field, E., Mead-Regan, S., Lowe, M., Kaski, J.P., 2017. Europace 19 (8), 1385–1391.
Park, J.S., Grijalva, S.I., Jung, D., Li, S., Junek, G.V., Chi, T., Cho, H.C., Wang, H., 2019. Biosens. Bioelectron. 144, 111626.
Sallam, K., Li, Y., Sager, P.T., Houser, S.R., Wu, J.C., 2015. Circ. Res. 116 (12), 1989–2004.
Shiroma, E.J., Lee, I.M., 2010. Circulation 122 (7), 743–752.
Sundarasekar, R., Thanjaivadivel, M., Manogaran, G., Kumar, P.M., Varatharajan, R., Chilamkurti, N., Hsu, C.H., 2018. J. Med. Syst. 42 (11), 228.
Tanaka, T., Tohyama, S., Murata, M., Nomura, F., Kaneko, T., Chen, H., Hattori, F., Egashira, T., Seki, T., Ohno, Y., 2009. Biochem. Bioph. Res. Co. 385 (4), 497–502.
van Meer, B.J., Krotenberg, A., Sala, L., Davis, R.P., Eschenhagen, T., Denning, C., Tertoolen, L.G.J., Mummery, C.L., 2019. Nat. Commun. 10 (1), 4325.
Wang, Q., Fang, J., Cao, D., Li, H., Su, K., Hu, N., Wang, P., 2015. Biosens. Bioelectron. 72, 10–17.
Wang, T., Hu, N., Cao, J., Wu, J., Su, K., Wang, P., 2013. Biosens. Bioelectron. 49, 9–13.
Woodcock, E.A., Matkovich, S.J., 2005. Int. J. Biochem. Cell Biol. 37 (9), 1746–1751.
Ye, Y., Guo, H., Sun, X., 2019. Biosens. Bioelectron. 126, 389–404.
Zhang, R., Wei, M., Chen, S., Li, G., Zhang, F., Yang, N., Huang, L., 2018. Biosens. Bioelectron. 110, 193–200.
Zhao, D., Liu, J., Wang, M., Zhang, X., Zhou, M., 2019. Nat. Rev. Cardiol. 16 (4), 203–212.